The Third Israeli Conference for Conveying and Handling of Particulate Solids
Joined with the Tenth International Freight Pipeline Society Symposium
Dead Sea, Israel, May 2000

APPLICATION OF TOMOGRAPHIC TECHNIQUES FOR IMAGING FLUIDIZED BEDS

T. Dyakowski and A.J. Jaworski
Department of Chemical Engineering, UMIST
PO Box 88, Manchester M60 1QD, UK

Abstract – This paper provides a review of the non-invasive techniques for studying fluidisation phenomena. These include optical photography, X-ray photography, X- and γ-ray tomography and capacitance tomography. Their specific attributes such as speed, sensitivity and robustness, are outlined and their potential for studying various aspects of gas-solids flow in different modes of fluidization is assessed. Finally a short case study on the monitoring of the flow inside a riser and a cyclone dipleg, using capacitance tomography, is presented.

1. INTRODUCTION

In the last few decades, since a successful introduction of fluidized bed technology, the instrumentation to monitor and quantify the fluidized bed operation has undergone several stages of development. In the most basic approach, the plant operation was controlled by measuring temperatures in selected places and the pressure drop along or simply across the bed. Clearly, these methods could only give superficial information, which could not be used in detailed flow analysis or plant troubleshooting.

Of course the spectrum of quantities, which need to be measured in a fluidized bed, is much wider. These include, for example, local solids volume concentrations, solids velocities and solids mass flows, the vertical and the horizontal distribution of solids inside the system or the lateral distribution of the fluidizing gas. In response to these needs a number of more sophisticated measurement techniques were proposed. For example, suction probes were developed to measure local solids and mass flow, heat transfer probes were proposed for detection of de-fluidized zones and solids flow inside fluidized-bed reactors. Other techniques include capacitance probes, optical probes, or γ-ray densitometry – a detailed review was given recently by Werther [1]

The above mentioned techniques, although much more useful than simple temperature and pressure measurements, which tend to treat the fluidized bed as a 'black box', have a major drawback of being point wise in character. The flow within the fluidized bed is fully three dimensional and is characterised by the formation, evolution and decay of large scale coherent structures, for example bubbles, or – in the micro-scale – the appearance of instabilities, such as strands or clusters of particles.

Therefore, understandably, significant effort was placed into developing the means of visualising and quantifying these phenomena in a non-invasive manner. These range from relatively simple

methods such as optical photography to more complex techniques such as tomography, which can provide both instantaneous and average distribution of gas and solids in the bed, as well as allow investigations of the temporal evolution of various flow instabilities. The measurement techniques discussed in this paper include optical photography, X-ray photography, X- and γ-ray tomography and capacitance tomography.

Generally speaking, photographic techniques provide a projection of flow patterns on a single plane, which in most cases is parallel to the fluidized bed axis. Tomographic techniques, on the other hand, provide a "cross-sectional" image of gas-solids distribution, obtained from a number of independent measurements (or "projections") performed on the boundaries of the imaging domain. The images can be obtained in planes, which are perpendicular or parallel to the fluidized bed axis.

2. PHOTOGRAPHIC METHODS

2.1 Optical photography

Optical photography is one of the simplest methods for studying fluidization phenomena. Very often, to avoid the effects of light reflection on a convex wall, the photographs are taken using 'two-dimensional' or semi-cylindrical columns (Figure 1). 'Two-dimensional' columns are of rectangular cross section, the width being considerably greater than the thickness. The fluidized particles are contained in the gap between the two flat, transparent faces, separated by a distance, which is usually in the range 10 to 25 mm.

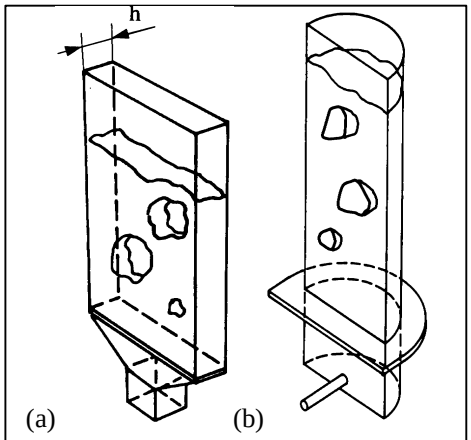

Figure 1. Schematic diagrams of
(a) – two dimensional column
(b) – semi-cylindrical column

Such columns have proved to be especially useful for studies of bubble properties and as a means of qualitatively viewing the fluidization characteristics of given powders [2-4]. Recently, Arena *et al*. [5] employed a thin, two-dimensional riser to visualise flow structures with a video system capable of 2000 frames per second.

While two-dimensional columns are useful for qualitative purposes, there are important quantitative differences between two- and three-dimensional fluidized beds. These arise from quantitative differences in rise velocities of isolated bubbles, different bubble coalescence properties, differences in bubble shapes and wake characteristics, jet stability in two-dimensional columns, different mechanisms of solids ejection into the freeboard, and reduced solids mixing. Rowe and Everett [6] studied the influence of the thickness, h, of a rectangular column of 0.30m width. The thickness was increased in stages from 14 mm (a two-dimensional column) to 0.30m (a fully three-dimensional column). For the range of conditions studied, there was a significant change in bubble properties for a thickness of less than about 0.10 m, with thickness having little discernible influence once this value was exceeded. The minimum column thickness (Lyall, [7]) is 30 mean particle diameters of spherical particles, but this ratio should be somewhat greater when the particles are angular, sticky, or have a broad size distribution.

A semi-cylindrical column is intermediate between a two-dimensional column and a cylindrical column and consists of a cylindrical vessel, which has been sliced in half, with a flat plate installed along the diametral plane (Figure 1b). In this case, front illumination is required for bubble viewing and photography, since bubbles generally do not span the entire bed thickness.

The use of this geometry is based on the assumption that one should view, through the flat face, the same processes, which would take place across the diameter of a full cylindrical column. Although this assumption is false from the fluid mechanical point of view the semi-cylindrical columns have been successfully used in spouted bed studies [8-10]. Rowe, Mac-Gillivray and

Cheesman [11] found that flat surfaces alter the behaviour of grid jets as compared with the case where the jet is centred in a fully cylindrical vessel – highlighting the concerns about the accuracy of measurements in semi-cylindrical columns.

Lyall [7] reported an application of optical photography for studying a bubble bursting on the surface of a fluidized bed. A bed 5.5 inches in diameter, 8 inches deep, with a porous bronze distributor was filled with a 3 inch layer of red Ballotini, then to within an inch of the top with white Ballotini. The bed was fluidized and a bubble ejected from the centre of the distributor. The lighting came from slightly behind the bubble so that the interior of the bubble was visible while it was bursting. Figure 2 shows two consecutive pictures taken from a 35mm ciné film at 32 frames per second.

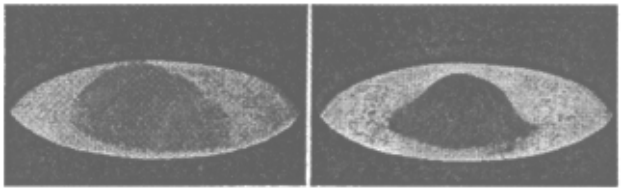

(a) (b)

Figure 2. Particle movement as a bubble bursts at the surface of a bed – shown by a short time exposure of 1/128th second: (a) bubble bursting, (b) bubble collapsing 1/32nd second later [7]

2.2 X-ray photography

Rowe, Yates and co-workers [12-15] have used X-ray photography to visualise flow patterns inside fluidized beds. The technique mimics the familiar medical X-ray transmission technique. Differences in density of the exposed subject appear as shadows on a photographic film. An important advantage is that images are recorded with high temporal resolution and can often reveal individual components of the bed structure. The investigations have been centred on the behaviour of gas bubbles in solid beds, phenomena such as bubble growth, bubble splitting (with and without the presence of internal heat exchanger tubes), the effects of gas distribution, elevated temperatures and pressures and co-axial nozzles.

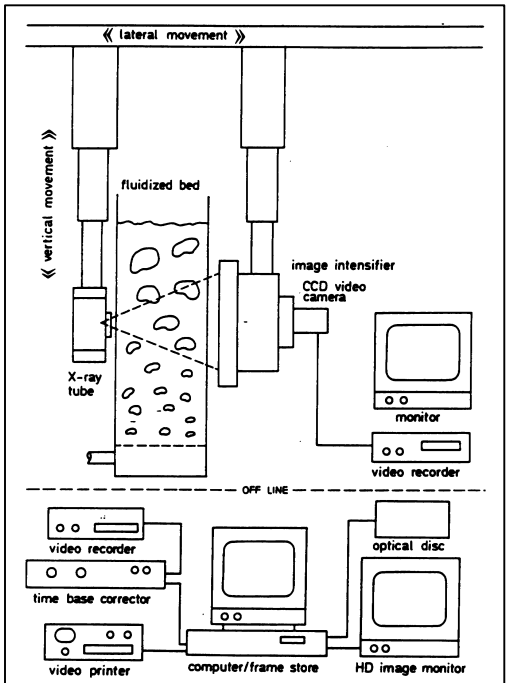

Figure 3. Schematic of the X-ray photography equipment at UCL [15]

The essential elements of the X-ray photography equipment are shown in Figure 3. The X-ray beam passes through the bed at a chosen level and images are captured by the video recorder at a rate of 25 frames per second. The recorder is synchronised with the X-ray source, which produces a pulse of energy of 1 ms duration. Each image is therefore effectively an instantaneous view. In a freely bubbling bed, there will be a degree of "shadowing" of bubbles in line with the beam. However, since the rise velocity of a bubble is a function of its size, two differently sized bubbles will generally separate as they rise through the field of view, thus enabling each to be observed.

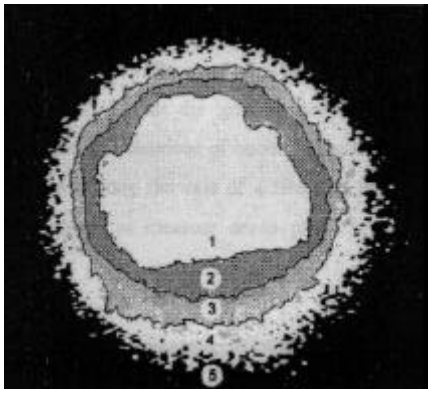

Figure 4. Voidage zones around a gas bubble in a fluidized bed of alumina [14]

An example of a computer-processed image of a single bubble rising through a bed of alumina is shown in Figure 4. The grey scale represents X-ray intensities in the zones of different porosity around the bubble. Two points need to be emphasised. Firstly, the computer is programmed to calculate

average values of voidage between any predetermined intensity values and to assign a grey scale accordingly; there is in fact a continuous gradation in voidage between one zone and the next. Secondly, the image is a representation in two dimensions of what is in reality a truly three-dimensional object (a silhouette), and therefore the voidage indicated is an average value across the chord of a more or less spherical region around the bubble. De-convolution techniques can be used on the silhouette to obtain point values of voidage, assuming that the three-dimensional object being considered is symmetrical relative to a vertical axis through its centre. To determine the gas content of the zones surrounding the bubble, such images are continuously calibrated during capture by relating the measured intensities to the two factors causing beam attenuation, namely: the path length of the beam through the powder and the solid density in the beam path. This is done by attaching to the side of the bed in the camera's field view a wedge-shaped vessel packed with the same powder as that comprising the fluidized bed. By equating the zone intensity with that at a given level of the wedge, the powder voidage can be determined [14].

3. TOMOGRAPHIC TECHNIQUES

3.1 gray tomography

γ-ray tomography evolved from earlier industrial applications of γ-ray densitometry, where a single collimated source of radiation and a single detector were used to establish the average density along the path of photon beam. The pioneering work in the area of γ-ray tomography is usually attributed to Bartholomew and Casagrande [16] (1957). They distributed four γ-radiation sources (5mCi ^{60}Co) around the bed periphery, together with eleven detectors (Geiger-Müller tubes) and obtained cross-sectional density contours from 18 “path measurements” using analytical methods (in fact the authors did not use the term “tomography” at that time). The sequence of measurements took approximately 1 hour.

Seville *et al*. [17] utilised the ?-ray technique to produce tomographic images of the voidage distributions of the jet region above various gas distributors and under different operating conditions. The system consisted of a single collimated photon beam and a single NaI detector aligned on an optical bench with the fluidized bed to be scanned (146 mm diameter, 200 mm in height) rotated and translated through the beam by a series of stepper motors. 40×2 mm steps were taken at 30×6° intervals with 1000 photons per ray-sum collected at each position.

Figure 5 illustrates one set of experiments carried out to investigate the effect of increasing gas velocity on jetting and bubbling behaviour. The bed particles were quartz sand (300-355 μm, U_{mf} =0.92 ms^{-1}) and the settled bed depth was 150 mm. The distributor was flat plate with 37 discrete orifices of 1.5mm diameter on a 24mm triangular pitch, giving a free area of 0.39%. Three different scanning heights were used (20, 30 and 40 mm above the distributor) at three gas velocities (1.38, 2.30 and 3.22 m s^{-1}). The tomograms produced by this technique clearly indicated the effects of process variables, such as background fluidization, particle angularity and gas velocity, on jet behaviour and allowed comparison of jet penetration lengths determined in this way to be made with those

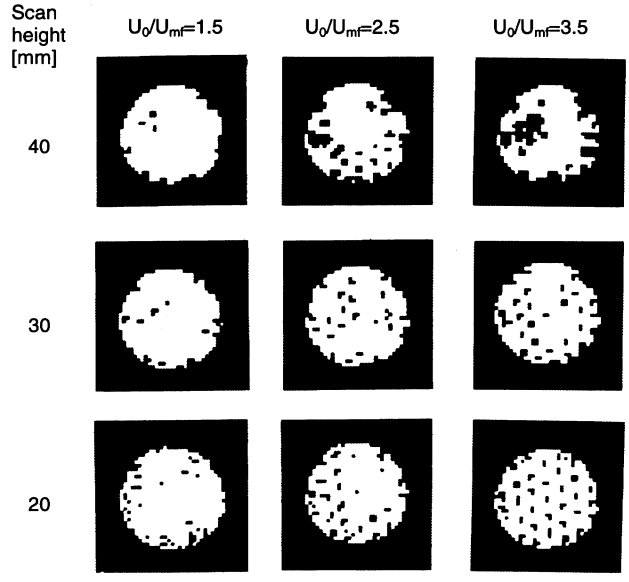

Figure 5 Binary images obtained from γ tomography [17]

predicted using well known correlations [18].

The results in 'binary' form (Figure 5) correspond to 9 combinations of experimental conditions. To facilitate comparison between the tomographic images, an attenuation threshold value was chosen (0.03 mm^{-1} corresponding to a voidage fraction of 0.525) below which all pixels were set to black, with the remainder to white. Regions of high average voidage are apparent at 20 and 30 mm above the distributor orifices with U_0/U_{mf}=3.22 and are also discernible at 20 mm with U_0/U_{mf}=2.30. The images show a decrease in the order of the structure with an increase in the scan height above the distributor, which is explained by degeneration of the jetting region into bubble flow. Similarly, the structural detail is increased at all heights as the velocity is increased due to an increase in the jet penetration lengths with increasing gas velocity.

Simons et al. [19] used an enhanced ?-ray tomography device to produce images of higher resolution at shorter scan times and with larger diameter vessels than those described by Seville *et al*. [17]. The "scanner" employed an array of six gadolinium-153 sources in conjunction with six collimated CsI scintillation detectors, all mounted on a fixed gantry with a circular opening through which a 100 mm (maximum) diameter cylindrical column could be lowered and raised. Instead of rotating the object to be scanned through the beam, the scanner ring was moved laterally in steps of 1.0 mm, each followed by a rotation of 1.5º around the object, until a full 180º rotation was completed. This resulted in reconstructed images made up of a 155 mm square grid of 1.0×1.0 mm^2 pixels and for full spatial resolution total scan times were kept around 3-4 h, although scan times of the order of 90 s could be achieved at cost of resolution.

More recently Turlier and co-workers [20-22] reported their work on industrial-scale processes. They developed a ?-ray device to obtain tomographic images and three-dimensional density maps of cross-sections in FCC risers. The preferred source for industrial applications is caesium-137 (500 mCi) with the detector being a lead collimated (30 mm diameter opening) NaI scintillator. The scanning apparatus can be used on objects up to 1.2m diameter and allows for any number of rotations and translations. Figure 6 shows a catalyst density map of an industrial riser, taken with three rotations by nine translations. In this case the solid mass flux is 1090 kg $m^{-2}s^{-1}$ and the superficial gas velocity is 25 m s^{-1}. The mean concentration near the wall is 270 kg m^{-3}, whilst the mean core concentration is 50 kg m^{-3}, i.e. the profile has a core-annulus structure. Generally 18 rotations and 11 translations have been used, complete scans taking up to 2 h. However, in practice 1-2 days are required to avoid any errors in interpretation. Other practical problems include the amount of space required for the equipment (e.g. for a riser of 1.1 m outer diameter, a free area of 2.3 m diameter is necessary) and the radiation hazard from the high intensity source. Such intensity is useful for obtaining good precision in counting rates, but operation of the device necessitates a delimited safety area and/or operation at night.

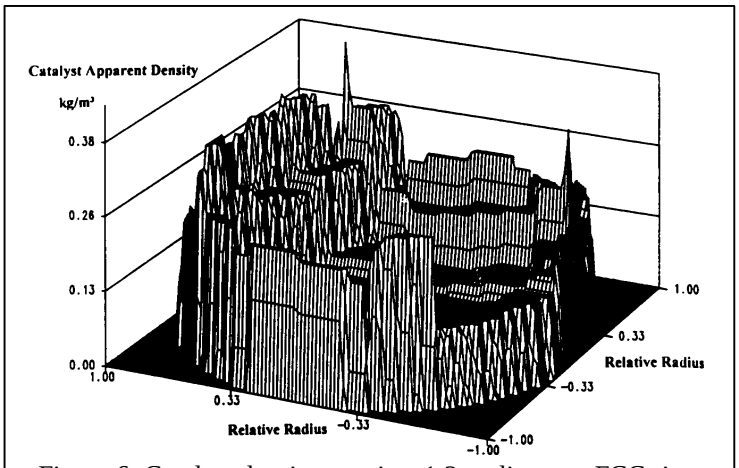

Figure 6. Catalyst density map in a 1.2 m diameter FCC riser determined by ?-ray tomography [21]

3.2 X-ray tomography

Unlike γ-ray tomography, where photons come as a result of spontaneous decays of atomic nuclei, in X-ray tomography the photons are generated in the so-called X-ray tubes. Here electrons are accelerated by a massive electrical potential between heated cathode and anode target. The

sudden stoppage of electrons on the target causes emission of X-rays with the energy typically between 50eV and 100keV. X-ray tomography became popular in fluidisation research after its successful application in the field of medical imaging. In the early 1980s large volumes of de-commissioned medical equipment became available for university use, which prompted extensive research work.

Banholzer *et al*. [23] described the use of medical X-ray tomography to directly observe the time-average flow pattern inside a laboratory scale fluidized bed made of a 150mm long polyacrylic tube with 43mm internal diameter and filled with pulverised coal. For coal, X-ray attenuation is dominated by Compton scattering so that visualisation is essentially that of the localised bed density to an excellent approximation. Spatial resolution is 0.087 mm^3, while density resolution is better than 30kg m^{-3}. Density differences within the confines of the fluidized bed were observed and quantified. Gradients in both the static and fluidized beds were observed. At the highest superficial velocity tested (0.288 m s^{-1}), channelling and/or a stream of bubbles along a central vortex region was noted. Wall effects were identified which would be obscured by visual examination. A general agreement between actual and expected flow patterns was found. Figure 7a shows the bed was well into the bubbling regime with 50-mm-high spouts visible at the top of the bed at a superficial velocity of 0.288 ms^{-1}. Figure 7b shows the density along a horizontal line measured from left to right.

Kantzas and co-workers [24-26] described the use of the X-ray tomography scanner, modified from its original medical use for chemical and petroleum engineering applications, to the study of fluidization. Perspex columns of 1 m in length and 5 cm to 30 cm in diameter were used in the experiments. A variety of high-density polyethylene, linear low-density polyethylene and impact polyethylene resins were used for the experiments.

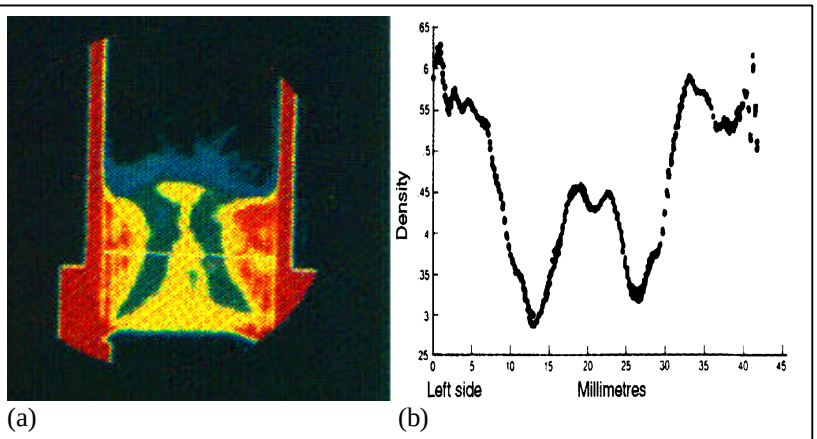

(a) (b)

Figure 7. (a) X-ray tomography image of fluidized bed (superficial velocity 0.288 ms^{-1}). (b) Solids density along a horizontal line [23]

An example of the results is shown in Figure 8. The images are taken, using resin M2, in a column with a diameter of 10 cm and at a fixed location – 3.6 cm from the distributor plate. The ratio of bed length to the bed diameter is 1. The settled bed image is shown on the left, while the fluidized bed image is shown on the right. A fairly uniform image is shown for the settled bed. There is somewhat lower voidage closer to the wall as opposed to that closer to the centre of the column. The fluidized bed image shows a very wide voidage distribution which has a lower voidage value at the wall (the top half of the image) while a high variability of the voidage values are shown in the lower part of the image with a typical cluster of bubbles appearing

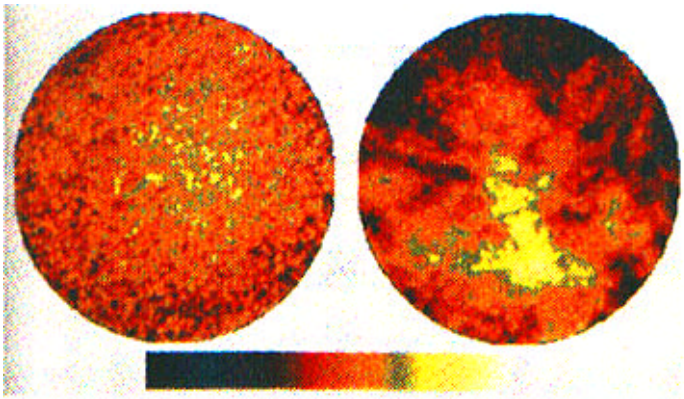

0.400000 voidage range; settled bed (left) 0.600000
0.400000 voidage range; fluidized bed (right) 0.800000

Figure 8. Voidage for settled (left) and fluidized bed (right) [25]

3.3 Capacitance tomography

Electrical Capacitance Tomography (ECT) systems have been developed relatively recently. Notably, researchers from Morgatown (WV, USA) have conducted a pioneering work in applying ECT to fluidisation research in the early 1990s [27,28]. Similar work at UMIST began shortly afterwards [29,30].

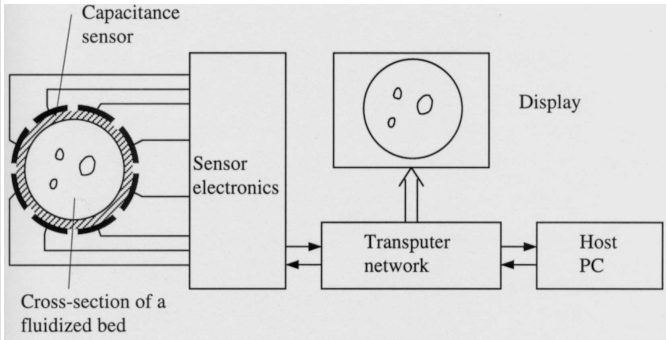

Figure 9. Typical sensor arrangement and data acquisition system for ECT imaging

A typical arrangement of the ECT system is shown in figure 9. A number of electrodes (here 8) are distributed around the test section. The electrical capacitance between all possible pairs of electrodes is measured and the image of solids concentration is obtained by processing the data using an appropriate reconstruction algorithm. From the viewpoint of the image resolution and the 'slice' thickness, the ECT systems are most certainly inferior to their nucleonic counterparts. Typical spatial resolution is 5-10% of vessel diameter with the electrode height of a few centimetres. Their advantage lies in fast imaging capabilities – e.g. for the UMIST system 200 frames per second, which outperforms most of the nucleonic systems used so far.

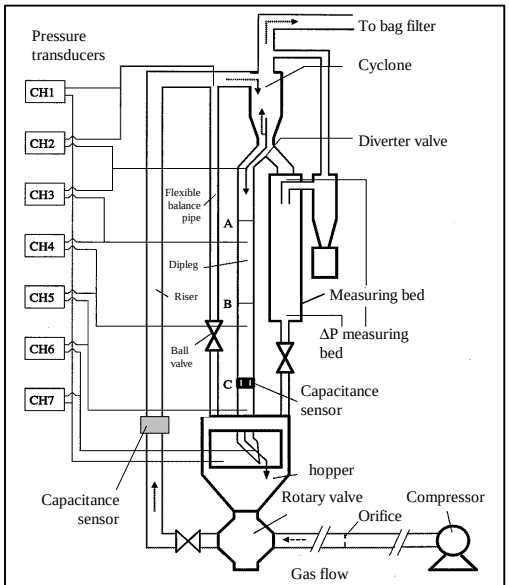

Figure 10. Experimental flow rig

The flow rig used in the presented study is shown in figure 10. The ECT sensor was placed in different locations along the riser and cyclone dipleg (A, B and C). The details of experimental procedures and results are given in [31]. Figure 11 shows a three-dimensional reconstruction of a 'train' of bubbles travelling through the bed close to the air distributor. It was obtained by stacking together a series of ECT measurements and setting an appropriate threshold on the voidage data. Of course, the vertical dimension is arbitrary as the ECT system had only a single plane.

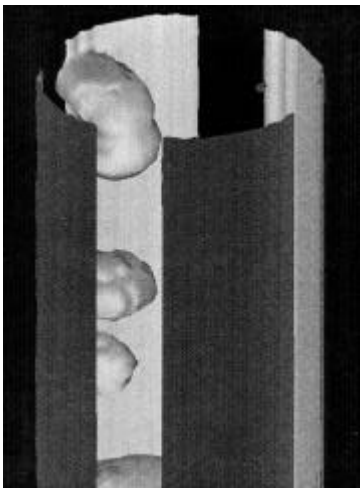
Figure 11. Three-dimensional reconstruction of the 'train' of bubbles

Examples of instantaneous images obtained within the dipleg are shown in figure 12. Letters E and F mark the projection of the common edge between the chute and the dipleg. The majority of instantaneous images obtained at level 'A' show that a region of high solids volume fraction exists around the EF. A region of low solids volume fraction was visible almost opposite this line. Occasionally, however areas of somewhat increased solids concentration can be seen opposite to line EF (t = 0.5, 1.0 and 3.0 s, for example). This seems to be caused by some fluctuations in the riser-dipleg system, which, in turn, generated an increase in solids velocity at the inlet to the dipleg.

Figure 13 shows averaged tomograms (obtained from 1000 consecutive frames) on all three levels A, B and C, for two solids flux values. It can be seen that solids falling down distribute themselves into a more annular shape around the wall. At the same time the solids concentration in the pipe centre increases.

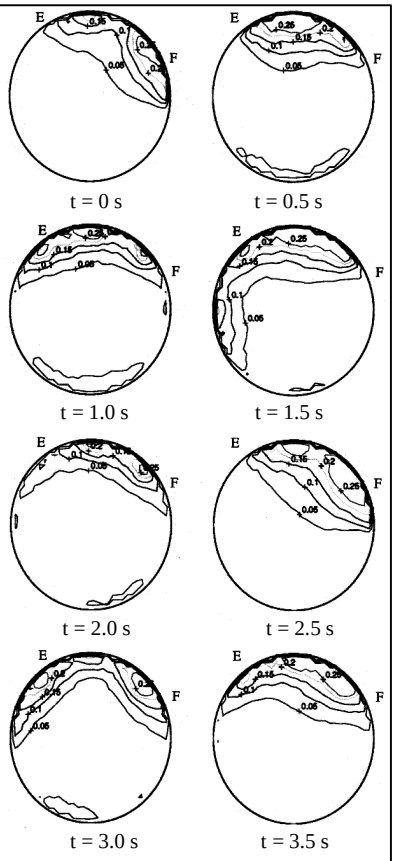

Figure 12. Instantaneous solids distribution in location A

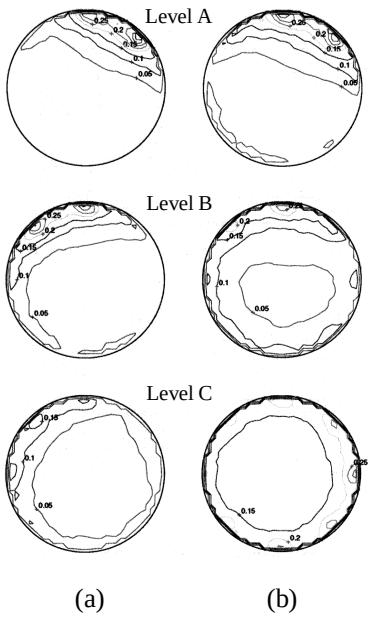

Figure 13. Time averaged solids volume fraction distribution: (a) solids flux G_s=111 kg m^{-2} s^{-1}, (b) solids flux, G_s=269 kg m^{-2} s^{-1}

4. SUMMARY

Imaging fluidization phenomena in a non-invasive manner is a challenging task. In the research environment the data obtained are important from the viewpoint of modelling of the complex gas-solids interactions, in addition to validation of numerical codes developed in recent years. In the industrial environment non-invasive techniques could be used for monitoring, control and 'troubleshooting' of the existing plants.

The 'ideal' characteristics of instrumentation to monitor fluidized beds can be obtained by a relatively simple dimensional analysis. Assuming that the dimensions of structures to be imaged are in the centimetre range and that characteristic flow velocities are between 1 and 10 ms^{-1} one can calculate characteristic time scale as 10^{-3} and 10^{-2} of a second. Furthermore, it could be assumed that in order to image the transient movement through the sensor one should be able to obtain a few (say 10) 'slices' of a given flow structure. This reduces the required imaging time to 1 – 0.1 of a millisecond, which in practical terms corresponds to between 1000 and 10000 frames per second.

Clearly, none of the imaging techniques presented here, at the current status of development, is capable of delivering such imaging speeds (an exception perhaps being high-speed cameras used in optical photography [5]). Despite these difficulties it has been shown that imaging of individual bubbles is achievable (see Figures 4 and 11) in the controlled laboratory environment.

From the material presented here it appears that at the current stage the nucleonic techniques can provide very good spatial resolution (down to fractions of a millimetre) but at a cost of lengthy data acquisition times (hours or minutes at best). On the other hand the electrical techniques, such as ECT, can offer relatively fast imaging (currently up to 200 frames per second) but with much poorer spatial resolution, typically 5-10% of the bed diameter.

These reasons limit the use of nucleonic tomography to obtaining average values, accurately in the spatial sense (Figures 5 – 8). On the other hand ECT is used as a 'crude' method of obtaining the solids concentration with fast data acquisition rates (see instantaneous images in Figure 12).

A poor spatial resolution is an inherent feature of electrical methods. This is due to the fact that the electrodes are of finite size as well as due to the 'soft field' effects present in the image reconstruction methods. It may be expected, however, that in future imaging speed could increase further thanks to better measurement electronics. Perhaps 1000 frames per second would be a reasonable expectation.

On the other hand, a slow performance of the nucleonic techniques is <u>not</u> a prerequisite. One has to remember that the methods of mechanical traversing of the source-detector arrangement around the objects were inherited from the earlier medical applications, where speed was not essential. The

work of researchers from the University of Bergen [32] shows clearly, that when the mechanical traversing is abandoned and instead multiple sources and detector arrays are used the imaging speed of a γ-ray tomography system can be increased to 25 frames per second. A similar concept is exploited by Morton et al. [33], who are currently developing an X-ray tomography system capable of providing images at 50 frames/per second. Although these numbers are still much less impressive than ECT the authors anticipate that perhaps 100-200 frames per second could be achieved. The issues to address this would certainly be connected to radiological safety.

It has to be emphasised that all techniques presented here have been successfully used in the research environment or pilot plant scale (γ-ray tomography). Their use in an industrial environment is a separate issue. One has to remember that commercial vessels may operate at high temperatures (say $700^{O}C$ – $850^{O}C$) and pressures, which may reach a few tens of bars. Their walls are made of steel and the vessel diameter may be within 1-5 m range. When such considerations are taken into account, the likelihood of using optical or X-ray in the process environment is rather small. A natural choice would be γ-ray techniques, which have a long history of industrial use. The prohibitive factor here could be the size of equipment and radiological hazards.

Application of ECT in industrial environment, in the authors' opinion, is difficult at the current stage, but not impossible. Clearly, the sensing electrodes would have to be placed inside the vessel, flush with the internal surface, but electrically insulated from the vessel wall. Perhaps ceramic inserts could be used for this purpose. Electrical connections would have to be engineered as pressure proof. Safety aspects such as electrostatic discharge should also be considered.

Table 1 gives a short summary of the current status of the measurement techniques presented in this paper, together with the authors' expectations as to the trends in their future evolution.

Table 1. Current status and author's expectations of the future development of non-invasive techniques

Methods	Data acquisition speed		Spatial resolution	Problems and issues to be addressed	Industrial use
	Current	Expected future improvements (5-10 years)			
Optical Photography	10,000 frames/s	No need	Down to fractions of a millimetre	Available light intensity	Unlikely
X-ray Photography	25 frames/s	100-200 frames/s (?) given that 1 ms bursts are already available	Down to fractions of a millimetre	Anode target overheating. Radiation health hazard	Unlikely due to X-rays not penetrating metal walls
X-ray Tomography	Minutes to hours per frame (medical equipment with mechanical traversing)	Abandon mechanical traversing. Use fixed multiple sources and detector arrays with fast electronics. 50 frames/s [33] 100-200 frames/s (?)	Down to fractions of a millimetre	Building powerful X-ray sources with short bursts. Anode target overheating. Radiation health hazards	Unlikely due to X-rays not penetrating metal walls
γ-ray Tomography	Minutes to hours per frame (mechanical traversing) 25 frames/s [32] (fixed sources and detector arrays)	Abandon mechanical traversing. Use fixed multiple sources and detector arrays with fast electronics. 100-200 frames/s (?)	Down to fractions of a millimetre	Use of powerful γ-ray sources. Radiation health hazard	Likely if radiation levels are acceptable. γ-ray densitometry already widespread.
Electrical (ECT)	200 frames/s	1000 frames/s (?)	5-10% of vessel diameter	Shorter measurement times (faster electronics)	Difficult. Electrodes to be installed inside vessels on a non-conductive layer. Pressure seal of electrical connections may be difficult. Electrostatic discharge needs addressing.

5. REFERENCES

1 Werther J 1999 Measurement techniques in fluidized beds, *Powder Technol*., **102**, 15-36

2 Hiraki I, Yoshida K and Kunii D 1966 Behaviour of bubbles in a two-dimensional fluidized bed, *Chem. Eng. Japan*, **4**, 139-46

3 Nguyen XT and Leung LS 1972 A note on bubble formation at an orifice in a fluidized bed, *Chem. Eng. Sci*., **27**, 1748-50

4 Lignola RG, Donsi G and Massimillla L 1983 Mass spectrometric measurements of gas composition profiles associated with bubbles in a two dimensional bed, *AIChE Symp. Ser*., **79** (222), 19-26

5 Arena U, Cammarota A, Marzocchella A and Massimila L 1989 Solids flow structures in a two-dimensional riser of a circulating fluidized bed, *J. Chem. Eng. Japan*, **22** (3), 236-41

6 Rowe PN and Everett DJ 1972 Fluidized bed bubbles viewed by X-rays, *Trans. Instn Chem. Engrs*,. **50**, 42-60

7 Lyall E 1969 The photography of bubbling fluidized beds, *Brit. Chem. Eng*., **14**, 501-6

8 Mathur KB and Epstein N 1973 *Spouted beds*, Academic Press, New York

9 Whiting KJ and Geldart D 1980 A comparison of cylindrical and semi-cylindrical spouted beds of coarse particles, *Chem. Eng. Sci*., **35**, 1499-1501

10 Geldart D, Hemsworth A, Sundavadra R and Whiting KJ 1981 A comparison of spouting and jetting in round and half-round fluidized beds, *Can. J. Chem. Eng*., **59**, 638-9

11 Rowe PN, MacGillivray HJ and Cheesman DJ 1979 Gas discharge from an orifice into a gas fluidized bed, *Trans. Instn Chem. Engrs*, **57**, 194-9

12 Rowe PN and Partridge BA 1965 An X-ray study of bubbles in fluidized beds, *Trans. Instn Chem. Engrs*, **43**, 157-65

13 Rowe PN and Yacono CXR 1976 The bubbling behaviour of fine powders when fluidized, *Chem. Eng. Sci*., **31**, 1179-92

14 Yates JG and Cheesman DJ 1992 Voidage variations in the regions surrounding a rising bubble in a fluidized bed, *AIChE Symp. Ser*., **88** (289), 34-9

15 Yates JG, Cheesman DJ and Sergeev YA 1994 Experimental observations of voidage distribution around bubbles in a fluidized bed, *Chem. Eng. Sci*., **49**, 1885-95

16 Bartholomew and Casagrande 1957 Measuring solids concentration in fluidized systems by gamma-ray absorption, *Industrial and Engineering Chemistry*, **49**(3), March, pp. 428-31

17 Seville JPK, Morgan JEP and Clift R 1986 Tomographic determination of the voidage structure of gas fluidized beds in the jet region, in *Fluidization V* (eds Ostergaard K and Sorensen A) Engineering Foundation, New York, 87-94

18 Massimilla L 1985 Gas jet in fluidized beds, in *Fluidization* (eds Davidson JF, Clift R and Harrison D), Academic Press, London, 133-72

19 Simons SJR, Seville JPK, Clift R, Gilboy WB and Hosseini-Ashrafi ME 1993 Application of gamma-ray tomography to gas fluidized and spouted beds, in *Tomographic Techniques for Process Design and Operation* (eds Beck MS, Campogrande E, Morris M, Williams RA and Waterfall RC), Computational Mechanics Publications, Southampton, 227-38

20 Azzi M, Turlier P, Bernard JR and Garnero L 1990 Mapping solid concentration in a circulating fluidized bed using gammametry, *Powder Technol*., **67**, 27-36

21 Martin MP, Turlier P and Bernard JR 1992 Gas and solid behaviour in cracking circulating fluidized beds, *Powder Technol*., **70**, 249-58

22 Desbat L and Turlier P 1993 Efficient reconstruction with few data in industrial tomography, in *Tomographic Techniques for Process Design and Operation* (eds Beck MS, Campogrande E, Morris M, Williams RA and Waterfall RC), Computational Mechanics Publications, Southampton, 285-94

23 Banholzer WF, Spiro CL, Kosky PG and Maylotte DH 1987 Direct imaging of time-averaged flow patterns in a fluidized reactor using X-ray computer tomography, *Ind. Eng. Chem. Res*., **26**, 763-67

24 Kantzas A 1994 Computation of holdups in fluidized and trickle beds by computer-assisted tomography, *AIChE J*., **40**, 1254-61

25 Kantzas A and Kalogerakis N 1996 Monitoring the fluidization characteristics of polyolefin resins using X-ray computer assisted tomography scanning, *Chem. Eng. Sci*., **51**, 1979-90

26 Kantzas A, Wright I and Kalogerakis N 1997 Quantification of channelling in polyethylene resin fluid beds using X-ray computer assisted tomography (CAT), *Chem. Eng. Sci*., **52**, 2023-35

27 Halow JS and Nicoletti P 1992 Observation of fluidized bed coalescence using capacitance imaging, *Powder Technol*., **69**, 255-77

28 Halow JS, Fasching GE and Nicoletti P 1993 Observation of a fluidized bed using capacitance imaging,*Chem.Eng.Sci*.,**48**, 643-59

29 Wang SJ, Dyakowski T, Xie CG, Williams RA and Beck MS 1995 Real time capacitance imaging of bubble formation at the distributor of a fluidized bed, *Chem. Eng. J*., **56**, 95-100

30 Dyakowski T, Wang SJ, Geldart D and Beck MS 1999 Tomographic studies of flow patterns within a circulating fluidized bed, *Chem. Eng. Comm*., **175**, 117-30

31 Wang SJ 1998 *Measurement of Fluidization Dynamics in Fluidized beds Using Capacitance Tomography*, PhD thesis, UMIST

32 Johansen GA, Frøystein T, Hjertaker BT and Olsen Ø 1996 A dual sensor flow imaging tomographic system, *Meas. Sci. Technol*., **7**, 297-307

33 Morton EJ, Luggar RD, Key MJ, Kundu A, Távora LMN and Gilboy WB 1999 Development of a high speed X-ray tomography system for multiphase flow imaging, *IEEE Trans. Nucl. Sci*., **46**(3), 380-84